Mon. Not. R. Astron. Soc. **338,** 253–262 (2003)

Extinction within 10° of the Galactic centre using 2MASS

C. M. Dutra,[1⋆] B. X. Santiago,[2] E. L. D. Bica[2] and B. Barbuy[1]

[1] *Universidade de São Paulo, Instituto de Astronomia, Geofísica e Ciências atmosféricas, CP 3386, São Paulo 01060-970, SP, Brazil*
[2] *Universidade Federal do Rio Grande do Sul, Instituto de Física, 91501-970 Porto Alegre, RS, Brazil*

Accepted 2002 September 5. Received 2002 August 26; in original form 2001 November 6

ABSTRACT

We extract J and K_s magnitudes from the 2MASS Point Source Catalog for approximately 6×10^6 stars with $8 \leqslant K_s \leqslant 13$ in order to build an A_K extinction map within 10° of the Galactic centre. The extinction was determined by fitting the upper giant branch of (K_s, $J - K_s$) colour–magnitude diagrams to a dereddened upper giant branch mean locus built from previously studied bulge fields. The extinction values vary from $A_K = 0.05$ in the edges of the map up to $A_K = 3.2$ close to the Galactic centre. The 2MASS extinction map was compared to that recently derived from DENIS data. Both maps agree very well up to $A_K = 1.0$. Above this limit, the comparison is affected by increased internal errors in both extinction determination methods. The 2MASS extinction values were also compared to those obtained from dust emission in the far-infrared using DIRBE/*IRAS*. Several systematic effects likely to bias this comparison were addressed, including the presence of dust on the background of the bulk of 2MASS stars used in the extinction determination. For the region with $3° < |b| < 5°$, where the dust contribution on the far side of the Galaxy is ≈5 per cent, the two extinction determinations correlate well, but the dust emission A_K values are systematically higher than those from 2MASS. A calibration correction factor of 76 per cent for the DIRBE/*IRAS* dust emission extinction is needed to eliminate this systematic effect. Similar comparisons were also carried out for the $1° < |b| < 3°$ and $|b| < 0.5°$ strips, revealing an increasing complexity in the relation between the two extinction values. Discrepancies are explained in terms of the calibration factor, increasing background dust contribution, temperature effects influencing the dust emission extinction and limitations in the 2MASS extinction determination in very high extinction regions ($|b| < 0.5°$). An asymmetry relative to the Galactic plane is observed in the dust maps, roughly in the sense that A_K values are 60 per cent smaller in the south than in the north for $1° < |b| < 5°$. This asymmetry is due to the presence of foreground dust clouds mostly in the northern region of the bulge.

Key words: dust, extinction – Galaxy: centre.

1 INTRODUCTION

The high extinction and its patchy distribution in the Galactic centre region have been a constant problem to the study of the properties of the bulge stellar population. Several efforts were carried out to investigate the extinction distribution close to the Galactic centre. For example, Catchpole, Whitelock & Glass (1990) studied the distribution of stars in the central $1° \times 2°$ of the Galaxy by means of J, H and K colour–magnitude diagrams (CMDs). They derived visual absorptions in the range $7 < A_V < 30$. Frogel, Tiede & Kuchinski (1999, hereafter FTK99) obtained extinction values varying from $A_V = 2.41$ up to $A_V = 19.20$ for 11 bulge fields with $|b| < 4°$, close to the Galactic centre. Stanek (1996) derived a mean extinction of $\langle A_V \rangle = 1.54$ for Baade's Window (Baade 1963). As a consequence, the investigations about the bulge stellar content based on optical data were restricted for a long time to lower-extinction regions such as Baade's Window.

The advent of near-infrared (NIR) surveys such as the Two Micron All Sky Survey (2MASS; Skrutskie et al. 1997) and the Deep NIR Southern Sky Survey (DENIS; Epchtein et al. 1997) has provided fundamental tools to study the stellar population (Unavane et al. 1998) and extinction (Schultheis et al. 1999) in the inner bulge. Recently, Dutra, Santiago & Bica (2002, hereafter Paper I) confirmed the existence of two new bulge windows, W0.2–2.1 and W359.4–3.1, closer to the Galactic centre than Baade's Window; they used the $J K_s$ photometry from the 2MASS survey archive to map the extinction distribution within 1° towards these windows. The reddening

⋆E-mail: dutra@astro.iag.usp.br

distribution in the bulge area is also fundamental to the understanding of the spatial distribution of globular clusters and their relation to the bulge field stellar population itself. Barbuy, Bica & Ortolani (1998) discussed the globular clusters projected within 5° of the nucleus and which appear to be related to the bulge, while Barbuy et al. (1999) discussed the properties of those found in the area covered by the present study.

In this work we use the 2MASS J (1.25 μm) and K_s (2.17 μm) photometric data to build (K_s, J–K_s) CMDs of bulge fields in order to map out the interstellar extinction in the central 10° of the Galaxy. The extinction was derived by means of the upper giant branch fitting method, similar to that described in Paper I. In Section 2 we revise this method and describe in detail the way we build the extinction map. In Section 3 we compare the present results with those from DENIS. In Section 4 we analyse the 2MASS and DIRBE/*IRAS* extinction maps, making use of simple models for the optical depth in different directions in the Galaxy, and discuss the asymmetries between observations in the northern and southern Galactic hemispheres. Finally, the concluding remarks are given in Section 5.

2 BUILDING THE EXTINCTION MAP WITH 2MASS DATA

In Paper I we have built an extinction map in regions of low-extinction by means of upper giant branch fitting. We adopted an upper giant branch template from a composite CMD using seven bulge fields from FTK99. Using this template we managed to reproduce the mean extinction in Baade's and Sgr I windows. Metallicity effects were not considered in Paper I, as Ramírez et al. (2000), from a spectroscopic study of central M giant stars, pointed out that there is no evidence for metallicity gradient within the inner bulge ($R < 560$ pc). Besides, FTK99 concluded that the amplitude of metallicity variations in the inner bulge implies very small giant branch slope changes. Therefore, we assume that the metallicity variations in the inner bulge do not significantly affect the extinction estimates and we use the same upper giant branch adopted in Paper I as a reference:

$$(K_s)_0 = -7.81(J - K_s)_0 + 17.83 \qquad (1)$$

The equation above appropriately describes the upper giant branch locus for stars with $8 \leqslant K_0 \leqslant 12.5$.

We carried out JK_s photometric extractions of stars in the 2MASS Point Source Catalog, available on-line http://irsa.ipac.caltech.edu/applications/Gator/, for 61 fields with radius $r = 1^\circ$ each. For most fields, we extracted stars in the range $8 \leqslant K_s \leqslant 11.5$, there being typically 60 000 such stars in each. For the fields with $|b| < 1.5^\circ$, we expected very high extinction (Schultheis et al. 1999); thus we extracted fainter stars, down to $K_s = 13$. This extra 1.5 mag allowed us to determine the best magnitude range for upper giant branch fitting, taking into account factors such as the increasing photometric errors and contamination by disc stars with fainter magnitude limits, and the decreasing observed extent of the upper giant branch in heavily reddened inner bulge fields. This issue is discussed in Section 2.1. In these low-latitude regions, the deeper 2MASS extractions led to a considerably larger number of stars per field, ≈200 000. Considering all the fields in the area, we extracted J and K_s magnitudes for approximately 6×10^6 stars. In order to map out the extinction in the 10° Galactic central region, we defined 961 cells with 4×4 arcmin^2 in size in each one of 61 extracted fields. The extinction was determined assuming that the upper giant branch defined by the stars in a cell has the same slope as that adopted as reference (equation 1). We then calculated the shift along the reddening vector necessary to make it fall onto the reference upper giant branch from the (K, J–K_s) values of each star. We used the relations $A_{K_s} = 0.670E(J - K_s)$ and $A_K/A_{K_s} = 0.95$ (Paper I) to derive the A_K values. The A_K adopted for each cell was taken to be the median of the distribution of A_K values for the individual stars in it; an iterative 2σ clipping was applied to the distribution of A_K values in order to eliminate contamination from foreground stars. Fig. 1. shows the method applied to a cell located at $\ell = 1.93^\circ, b = 0.93^\circ$; the stars in the observed CMD (open circles) have a median extinction of $A_K = 0.74$ with respect to the reference upper giant branch. The extinction-corrected CMD based on this value is also shown (filled circles) in the figure. Note that the extinction-corrected CMD is well fitted by the reference upper giant branch (straight line), indicating that the determined median extinction is representative of most stars within the cell's area.

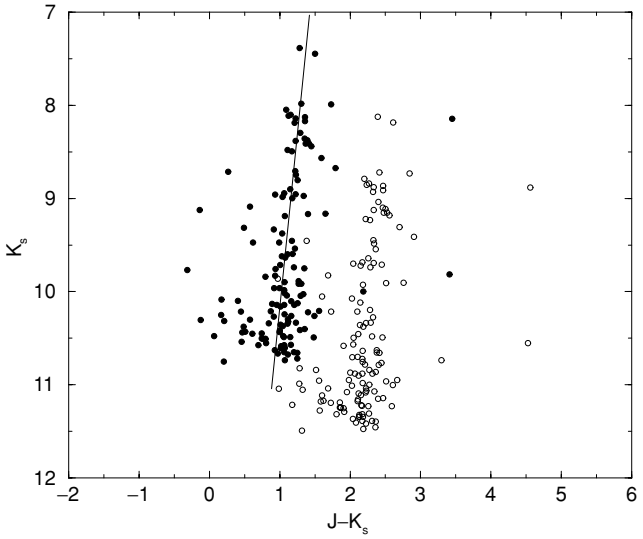

Figure 1. Extinction-corrected (filled circles) and observed (open circles) CMDs for a cell at $\ell = 1.93^\circ, b = 0.93^\circ$. The straight line represents the reference upper giant branch (equation 1).

2.1 The upper giant branch fitting in heavily reddened fields

We now try to assess the existence of systematic effects on the extinction determination just outlined. Pushing the limits used in our fitting method towards fainter magnitudes is desirable only if it increases the magnitude range where the upper giant branch is clearly defined and can be fitted. Several factors may prevent fainter magnitudes from being useful in this way. The first is obviously the increasingly large photometric errors. The 2MASS JK_s nominal errors are smaller than 0.04 for $J \lesssim 15$ and $K_s \lesssim 11.5$. Close to the centre, however, the density of stars increases very rapidly, yielding less precise photometric measurements due to source crowding. Another issue is the existence of selection effects: we fit a straight line to the upper giant branch defined in a (K_s, $J - K_s$) CMD. The K_s limit to the data will stand out clearly as a lower limit in the populated CMD region, but any J band cut-off will be a diagonal line on the CMD. It will bias our best-fit line if the giant branch is crossed by this diagonal line within the magnitude range used in the fit. Finally, at fainter magnitudes the bulge luminosity function rises rapidly, increasing the contamination by bulge stars with less

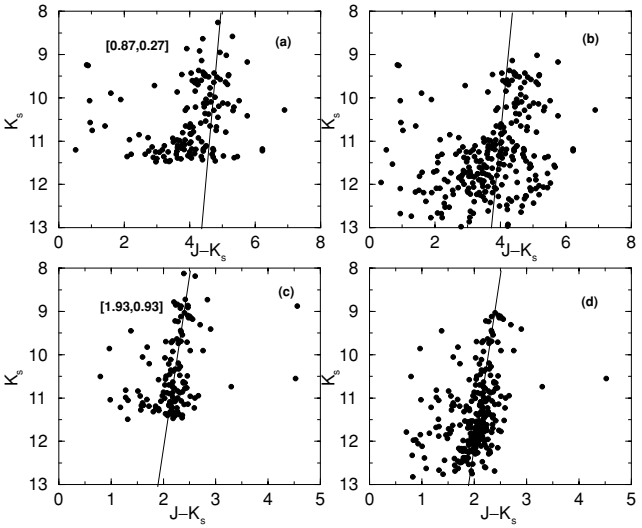

Figure 2. Analysis of limiting magnitude for fields with $|b| < 1.5^\circ$: CMDs for stars with (a) $8 \leqslant K_s \leqslant 11.5$ and (b) $9 \leqslant K_s \leqslant 13$ within a cell at $\ell = 0.87^\circ$, $b = 0.27^\circ$; (c) and (d) same K_s intervals as in (a) and (b), for stars within a cell at $\ell = 1.93^\circ$, and $b = 0.93^\circ$, respectively. The straight line represents the reddened reference upper giant branch. The derived extinction values in panels (a) and (b) are $A_K = 1.88$ and 1.83, respectively. For (c) and (d), $A_K = 0.74$.

extinction than the average, which will hamper our attempt to fit the bulk of the bulge stellar population.

All the three factors just mentioned are in fact present in our data to some extent. Fig. 2. shows the CMDs for two sample cells: one at $\ell = 0.87^\circ$, $b = 0.27^\circ$ (panels a and b), the other at $\ell = 1.93^\circ$, $b = 0.93^\circ$ (panels c and d). The panels on the left (right) show the data in the range $8 \leqslant K_s \leqslant 11.5$ ($9 \leqslant K_s \leqslant 13$). The reference upper giant branch is shown in all panels, reddened by the best-fitting $[A_K, E(J-K)]$ value found in each case. Clearly, the extinction is underestimated for the lower latitude cell when stars in the $9 \leqslant K_s \leqslant 13$ interval are used. The reason for that is two-fold: there is a large number of blue stars with $K_s \gtrsim 11$ and there is a paucity of stars in the lower right corner of the CMD in Fig. 2(b). Both tend to shift the best-fitting line towards the blue.

The scarcity of faint red stars is due to the 2MASS J-band limit: there are essentially no stars beyond the diagonal line $J = 16.5$, which is thus the 2MASS Point Source Catalog limiting J magnitude. This empirical limit is close to that proposed by the 2MASS collaboration (Skrutskie et al. 1997, see also the 2MASS web site). The faint blue stars are probably due to contamination from bulge stars with less extinction and to the increased photometric errors in these dense fields.

Note that the fit within the range $8 \leqslant K_s \leqslant 11.5$, despite the inclusion of some residual stars bluewards of the giant branch, is not biased (Fig. 2a). For the cell at $\ell = 1.93^\circ$, $b = 0.93^\circ$ the situation is more reassuring, the derived A_K being insensitive to the magnitude range used. We thus conclude that a more efficient use of the CMDs in the crowded and high extinction areas close to the Galactic plane is made by restricting the fit to $K_s = 11.0$. This limit is also conveniently close to where completeness effects should start to be significant in the 2MASS. For DENIS, Unavane et al. (1998) estimated the 80 per cent completeness level to be at $K \simeq 10$; $J \simeq 13$ and the 2MASS data are about 1 mag fainter.

We conclude that in areas where extinction is around $A_K \leqslant 1.5$ and photometric errors are not substantially increased by crowding our fitting method does not suffer from any biases due to the J band cut-off. For $A_K \simeq 2.5$, the J band detection limit effects become dominant and the range available for the fit is substantially shortened, rendering the extinction determination unreliable.

2.2 The A_K extinction map

Fig. 3 shows the A_K contour map for the central $10^\circ \times 10^\circ$ of the Galaxy obtained by applying the method described in the previous section to stars down to $K_s = 11.0$. The A_K contours show that the regions with $A_K > 1.5$ are concentrated in the area with $|b| < 1^\circ\!.0$. The isocontours with high values are slightly asymmetric with respect to the mid-plane and more extended in the southern hemisphere. They appear to be caused by the displaced location of the Sun from the plane (Section 4). The structure with extinction values between $A_K = 0.5$–1.0 and angular dimension of $3^\circ \times 2^\circ$ around $\ell = 1.5^\circ$ and $b = 4.0^\circ$ is a component of the Pipe Nebula, a dark nebula recently studied in CO by Onishi et al. (1999). This nebula appears to be located at 160 pc from the Sun, as a southern extension of the Ophiuchus dark cloud complex, and is located at the edge of the ScoOB2 association (Onishi et al. 1999). The detection of the Pipe Nebula in Fig. 3 suggests that nearby clouds cannot be neglected in attempts to interpret central extinction maps. From the 32 761 cells that cover a $12^\circ \times 12^\circ$ central area of the Galaxy, we have 2MASS data for 80 per cent of them. The quadrant $0^\circ < \ell < 5^\circ$, $-5^\circ < b < 0^\circ$, which comprises Baade's Window, is so far only partially released by 2MASS.

Fig. 4 shows a histogram of A_K values for the cells in the $10^\circ \times 10^\circ$ extinction map. The mean extinction in the entire map is $\langle A_K \rangle = 0.29$ with a standard deviation $\sigma = 0.12$ from the mean. 63 per cent of the cells fall within 2σ of this mean value, and 80 per cent of them have $A_K < 1.0$. The upper panel of Fig. 5. shows the histogram of internal errors in extinction determination. The mean internal error is $\langle \sigma_i \rangle = 0.08$, with a standard deviation of 0.02 around this mean. 70 per cent of the cells have internal errors within 2 standard deviations from the mean value ($0.04 \leqslant \sigma_i \leqslant 0.12$). The lower panel shows the dependence of internal errors with A_K; we note that for $A_K > 1.5$ the internal errors increase significantly.

As the present extinction map can be useful for a wide variety of Galactic and extragalactic studies in such central directions, it will be provided in electronic form in the CDS, by columns: (1) and (2) galactic longitude and latitude of the cell centre, (3) the K-band extinction A_K and (4) the uncertainty in the A_K determination σ_i.

3 A 2MASS VERSUS DENIS EXTINCTION COMPARISON

Schultheis et al. (1999) provided an extinction map for the inner Galactic bulge (covering $|\ell| < 8^\circ$ and $|b| < 1.5^\circ$) obtained from the J and K_s DENIS CMDs, together with isochrones from Bertelli et al. (1994), hereafter called the DENIS extinction map. The differences between the present extinction determination applied to 2MASS photometry and the procedure adopted by Schultheis et al. (1999) are the following: (i) the latter use an isochrone from Bertelli et al. (1994), with metallicity $Z = 0.02$, age of 10 Gyr and distance $d =$ 8 Kpc, to represent the dereddened (K, J–K) CMD of the bulge fields; (ii) Schultheis et al. adopt a transformation from K to K_s with an estimated error of 0.04 mag, in order to be able to use isochrone fitting; and (iii) the DENIS infrared photometry is limited to $K_s = 11.0$, with detection limits at $J = 16.0$ and $K_s = 13.0$ (Schultheis et al. 1999).

Unavane et al. (1998) estimated a DENIS completeness limiting magnitude of $K_s = 10.0$ in the inner bulge. The resolution of

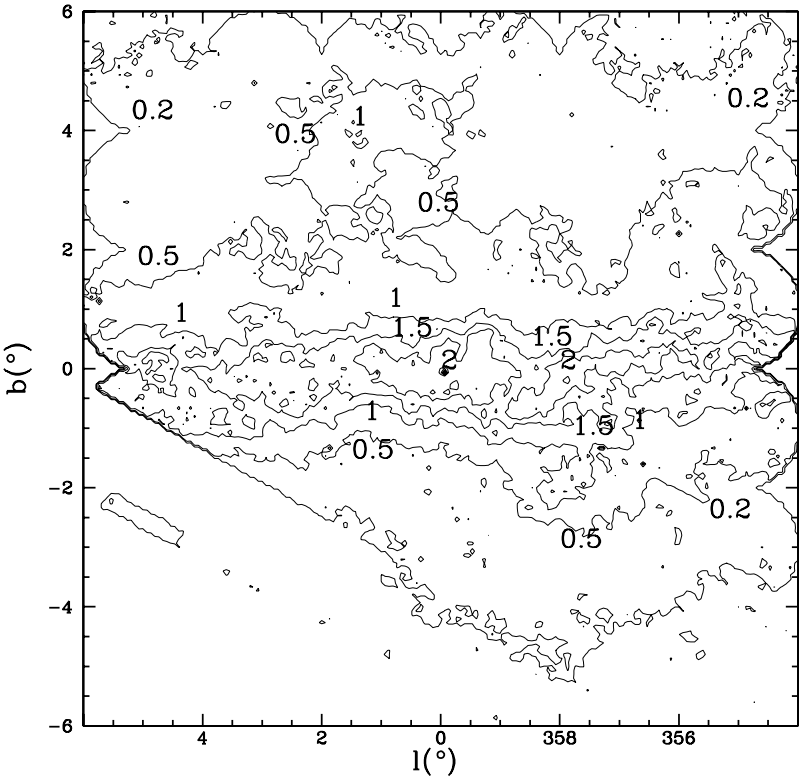

Figure 3. $A_{K,2MASS}$ extinction map within $10^\circ \times 10^\circ$ of the Galactic centre. The contours represent the following extinction values: $A_K = 0.2$, 0.5, 1.0, 1.5 and 2.0.

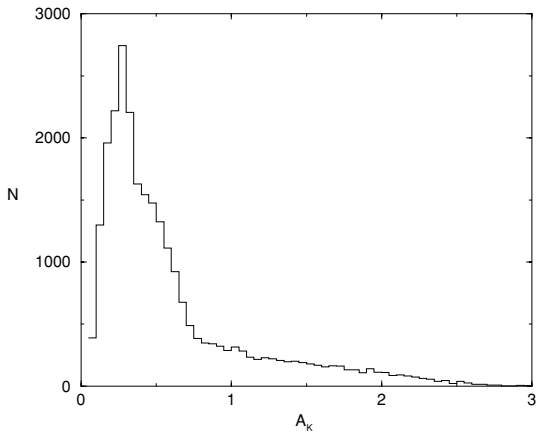

Figure 4. Histogram of A_K extinction values of the 10° extinction map.

the DENIS extinction map is also 4 arcmin. Fig. 6. shows the comparison of the extinction values derived from the 2MASS photometry, $A_{K,2MASS}$, with those derived from the DENIS photometry, $A_{K,DENIS}$, for the area in common between the two maps ($|\ell| < 5^\circ$ and $|b| < 1.5^\circ$). The extinction values derived from the 2MASS and DENIS photometric data present an excellent agreement, especially up to $A_K = 1.0$. Beyond this limit $A_{K,DENIS}$ values are higher than $A_{K,2MASS}$ ones, but if we consider that the uncertainties in the extinction determination and photometric errors increase in these zones, the agreement is still significant. The departure from identity line in Fig. 6 could be partially due to differences

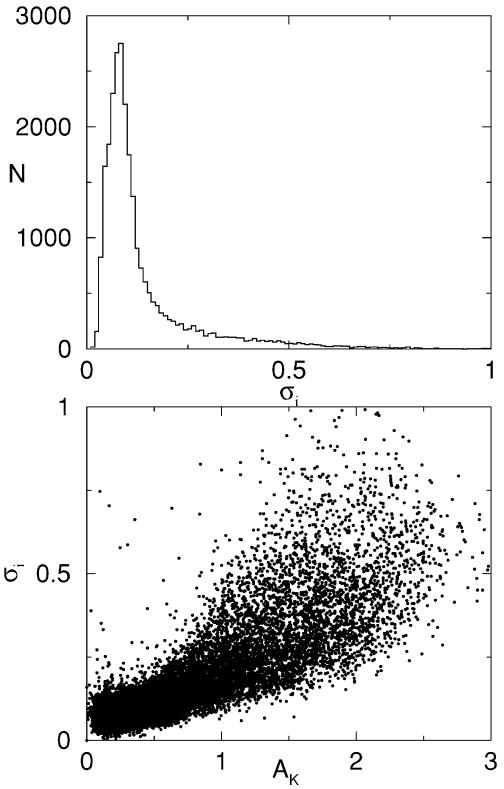

Figure 5. Upper panel: histogram of internal error σ_i values. Lower panel: variation of σ_i with A_K extinction values.

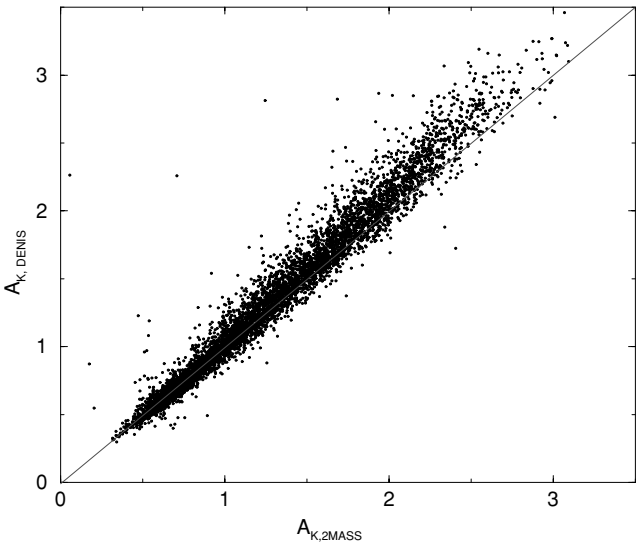

Figure 6. Comparison between $A_{K,\mathrm{2MASS}}$ and $A_{K,\mathrm{DENIS}}$ extinction values for the region $|\ell| < 5^\circ$ and $|b| < 1.5^\circ$. The straight line represents the identity function.

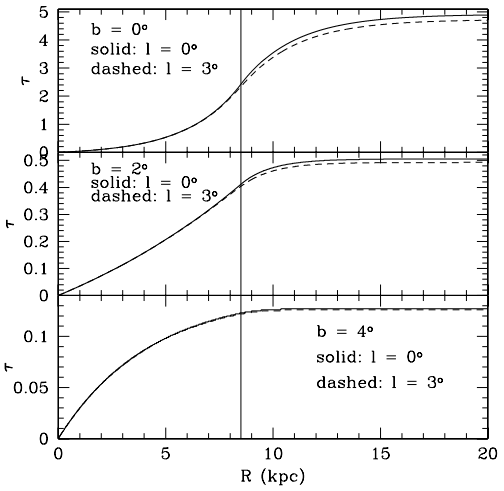

Figure 7. Increase in optical depth as a function of distance from the Sun as predicted by a simple model for the dust distribution in the Galaxy. The upper panel shows directions along the disc plane, for two values of longitude l, as indicated. The middle (lower) panel shows directions with $b = 2^\circ$ (4°).

in the filter profiles and zero-point calibrations adopted by the two surveys.

4 A 2MASS VERSUS FAR-INFRARED (FIR) EXTINCTION COMPARISON

Schlegel, Finkbeiner & Davis (1998) (hereafter SFD98) presented an all-sky reddening map based on the 100-μm dust emission, modelling the emission by dust grains with blackbody radiation at a temperature $T = 18.2$ K. Temperature corrections were applied by means of the 100- and 240-μm DIRBE maps, up to $T = 21$ K and in low angular resolution (1°). Their $E(B-V)_{\mathrm{FIR}}$ values correspond to the integrated dust column contribution throughout the Galaxy. The transformation from $E(B-V)_{\mathrm{FIR}}$ to $A_{K,\mathrm{FIR}}$ assumed $A_K = 0.112 A_V$ and $R_V = A_V/E(B-V) = 3.1$ (Cardelli, Clayton & Mathis 1989). The 2MASS extinction values, on the other hand, are based on the position of bulge red giant stars in the CMD and, as such, are limited in depth by opacity effects in the employed bands, especially in the J band.

In this section we compare the A_K extinction values derived from dust emission, $A_{K,\mathrm{FIR}}$, to those from the 2MASS photometry, $A_{K,\mathrm{2MASS}}$. However, before we can properly compare these two extinction maps, we must first investigate the possible existence of systematic effects on this comparison, such as variations in dust temperature and line of sight distribution or the presence of high density intervening clouds. Such effects should arise due to the widely different observational signatures from the interstellar medium on which the two extinction values are based.

4.1 Foreground dust versus background dust

In order to help interpreting the relation between $A_{K,\mathrm{2MASS}}$ and $A_{K,\mathrm{FIR}}$, we consider a simple model of dust distributed exponentially along and perpendicular to the Galactic plane. The optical depth out to some distance r from the Sun in the direction given by Galactic coordinates (ℓ, b) is then:

$$\tau(r, l, b) \propto \int_0^r \mathrm{e}^{-R(r,l,b)/R_\mathrm{d}} \mathrm{e}^{-|Z(r,b)|/Z_\mathrm{d}}, \qquad (2)$$

where $Z = r \sin b$ and $R^2 = R_0^2 + r^2 \cos^2 b - 2R_0 r \cos b \cos \ell$ are cylindrical coordinates centred on the Galaxy. R_d and Z_d are the dust horizontal and vertical exponential scales, whose values we assume to be 2.5 kpc (Robin et al. 1996 and Drimmel & Spergel 2001) and 110 pc (Mendez & van Altena 1998), respectively. We also adopt $R_0 = 8.5$ kpc for the Sun's distance from the centre of the Galaxy. We numerically performed the integral above for the same directions for which we have 2MASS and DIRBE/*IRAS* data. For each direction, we assume that our model $A_{K,\mathrm{2MASS}}$ and $A_{K,\mathrm{FIR}}$ values are proportional to $\tau(R_0)$ (hereafter $\tau_{8.5}$) and $\tau(\infty)$ (hereafter τ_∞), respectively. To model the foreground and background distribution with respect to the Galactic centre, we also assume that the Solar position is displaced by $Z_\mathrm{sun} = 15$ pc above the Galactic plane (e.g. Cohen 1995); in the double exponential dust distribution model, the fraction of foreground-to-total dust distribution does not depend on whether the Sun is displaced above or below the Galactic plane. A full data versus models comparison is currently under way. For now we restrict our discussion to the basic model features and their differences relative to the data.

Fig. 7. shows τ as a function of distance from us for several directions (l, b) as predicted by our simple model. The figure clearly shows the dependence on Galactic latitude of the expected contribution of dust beyond $R_0 = 8.5$ kpc. The fraction of the total optical depth caused by dust beyond the Galactic centre varies from 50 per cent at the Galactic plane to only a few percent for $b = 4^\circ$. Fig. 7 also shows that the total optical depth itself decreased by nearly two orders of magnitude between these two Galactic latitudes. The dependence on ℓ, on the other hand, is quite small.

4.2 Resolution elements and zones of avoidance

As we determined $A_{K,\mathrm{2MASS}}$ in cells of 4 arcmin on a side, the resolution of our maps is larger than the 6.1-arcmin resolution of the SFD98 extinction maps. In order to place both maps on a similar angular resolution, we convolve the $A_{K,\mathrm{2MASS}}$ extinction map with a $\sigma = 4.5$ arcmin Gaussian.

However, there are biases that do not depend on the resolution scale of the maps. One important issue is that the $A_{K,\mathrm{2MASS}}$ values require a minimum number of stars along the upper giant branch

to be determined. Regions with $A_K \gtrsim 2$ may be obscured enough that only the brightest stars will fall in the range $K_s \leqslant 11$ used to determine $A_{K,\mathrm{2MASS}}$ (see Section 2.1). If the region covers the entire cell, then no extinction value will result. However, more common will be the cases when this zone of avoidance partially covers a cell. In that case, the cell may still have stars enough for the giant branch fitting method to be applied, but the resulting $A_{K,\mathrm{2MASS}}$ will be an underestimate of the true one. Note that the $A_{K,\mathrm{FIR}}$ values will not suffer from such bias. We may model the latter simply as an average over the entire cell:

$$\tau_{\mathrm{FIR}} = \frac{\int_{\mathrm{cell}} \tau(\omega)\,\mathrm{d}\,\omega}{\int_{\mathrm{cell}} \mathrm{d}\,\omega}$$

where the integral is over the cell's solid angle and $\tau(\omega)$ is the varying K-band optical depth within the cell boundaries. For the 2MASS, assuming that only regions with $\tau < 2$ will contribute with CMD stars, we would have:

$$\tau_{\mathrm{2MASS}} = \frac{\int_{<2} \tau(\omega)\,\mathrm{d}\,\omega}{\int_{\mathrm{cell}} \mathrm{d}\,\omega}$$

where the 2MASS integral limit on the numerator corresponds to the cell regions where $\tau < 2$. We may then estimate the relative bias in the latter quantity by determining the ratio $\tau_{\mathrm{2MASS}}/\tau_{\mathrm{FIR}}$ for some model for $\tau(\omega)$. An important case of interest, especially for the lowest b regions ($|b| < 0.5^\circ$; see Fig. 3), will be that of a direction cutting through a dense dust cloud. We may consider that the cloud will dominate the dust column density in that direction and therefore ignore the contribution of foreground and background material. If we also assume the cloud to have a central optical depth τ_0, circular symmetry, and an exponentially falling dust column density, we will have:

$$\tau(\omega) = \tau(\theta) = \tau_0 \mathrm{e}^{-\theta/\theta_0}$$

where θ is the angle between the direction to the cloud centre and the direction considered and θ_0 is the cloud exponential scale.

Fig. 8 shows $\tau_{\mathrm{2MASS}}/\tau_{\mathrm{FIR}}$ as a function of τ_0 for several choices of θ_0. For $\theta_0 = 2$ arcmin and $\tau_0 > 5$, the entire cell would have $\tau > 2$ and therefore $\tau_{K,\mathrm{2MASS}}$ would become undetermined. We infer from the figure that the bias on the 2MASS data is relatively insensitive to the cloud profile shape but it is clearly dependent on profile normalization. For dust clouds with $\tau_0 < 5$ (roughly corresponding to a central $A_V < 55$), the systematic effect on $A_{K,\mathrm{2MASS}}$ will be $\lesssim$20 per cent. Note that these ratios were computed assuming the centre of the dust cloud to coincide with the centre of the cell. For the more common off-centre positions, $A_{K,\mathrm{2MASS}}/A_{K,\mathrm{FIR}} \simeq \tau_{K,\mathrm{2MASS}}/\tau_{\mathrm{FIR}}$ will be larger than shown in Fig. 8. Also, in the higher extinction regions there may possibly be more than one cloud per cell, thus increasing this systematic effect.

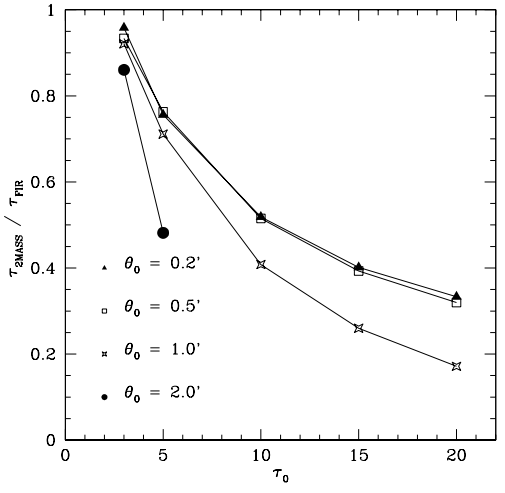

Figure 8. Relative loss of sensitivity in the 2MASS extinction determination method due to high density intervening dust clouds. The optical depths are assumed to be averages over the entire cell of 6.1 arcmin in side. The cloud column density profile is assumed to be exponential, with scale length θ_0 and central column density τ_0. τ_{FIR} is averaged over the entire cell but the 2MASS value is assumed to be restricted only to points with $\tau \leqslant 2$. The ratio $\tau_{\mathrm{2MASS}}/\tau_{\mathrm{FIR}}$ is plotted against τ_0 for different values of θ_0, as indicated.

4.3 $A_{K,\mathrm{2MASS}}/A_{K,\mathrm{FIR}}$ ratio map

Fig. 9 shows a grey-scale map of the $A_{K,\mathrm{2MASS}}/A_{K,\mathrm{FIR}}$ ratio, which provides information about the relative contribution of dust on the background of the Galactic centre, as background dust affects only $A_{K,\mathrm{FIR}}$. Since this is a ratio map between two observed extinction distributions, the result is not dependent on the calibration details. We note a global effect in the sense that $A_{K,\mathrm{2MASS}} < A_{K,\mathrm{FIR}}$, which will be discussed later. One clearly sees from the ratio map the existence of a flat region of very low $A_{K,\mathrm{2MASS}}/A_{K,\mathrm{FIR}}$ ratio. In this region closest to the plane, the FIR extinction values reach much larger optical depths than the 2MASS data. Besides, the FIR extinction values are severely overestimated by FIR emission of dust heated at temperatures above those assumed in the correction based on the 100- and 240-μm DIRBE maps. There are also two symmetric dark regions close to the Galactic centre, where $A_{K,\mathrm{2MASS}}$ is comparable to $A_{K,\mathrm{FIR}}$. These structures suggest a conical region depleted of dust on either side of and centred at the nucleus. This interpretation is based on the more limited optical depth of the 2MASS extinction values, and on the fact that the features on the foreground of the Galactic centre are present both in the 2MASS and FIR maps and should therefore be cancelled out. This conical structure is similar to those observed in emission line maps from some AGNs (e.g. Storchi-Bergmann & Bonatto 1991). It might be related to the central low-luminosity AGN in our Galaxy, with an ionizing cone orientation nearly coincident with that of the Galaxy

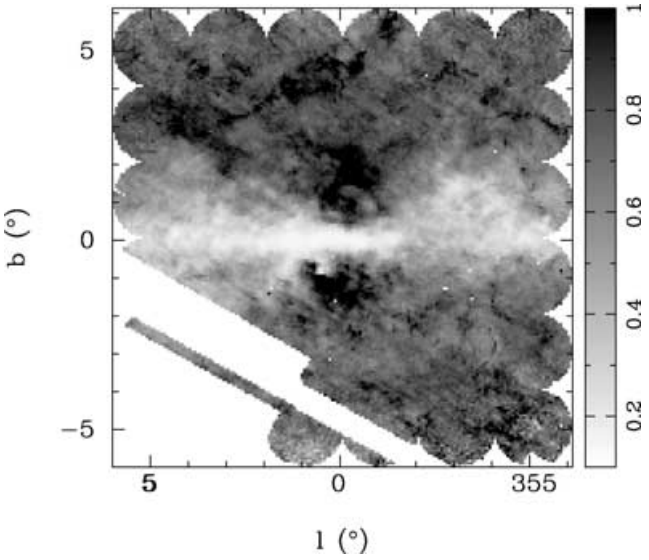

Figure 9. $A_{K,\mathrm{2MASS}}/A_{K,\mathrm{FIR}}$ ratio map within $10^\circ \times 10^\circ$ of the Galactic centre. Large (small) ratio values correspond to dark (light) areas as indicated in the grey-scale bar shown on the right.

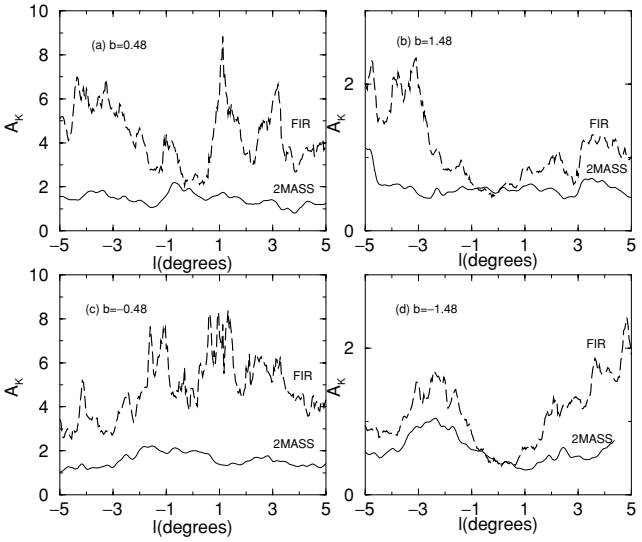

Figure 10. $A_{K,\mathrm{2MASS}}$ (solid line) and $A_{K,\mathrm{FIR}}$ (dashed line) profiles in galactic longitude centred in the galactic latitudes: (a) $b = 0.48°$, (b) $b = 1.48°$, (c) $b = -0.48°$ and (d) $b = -1.48°$.

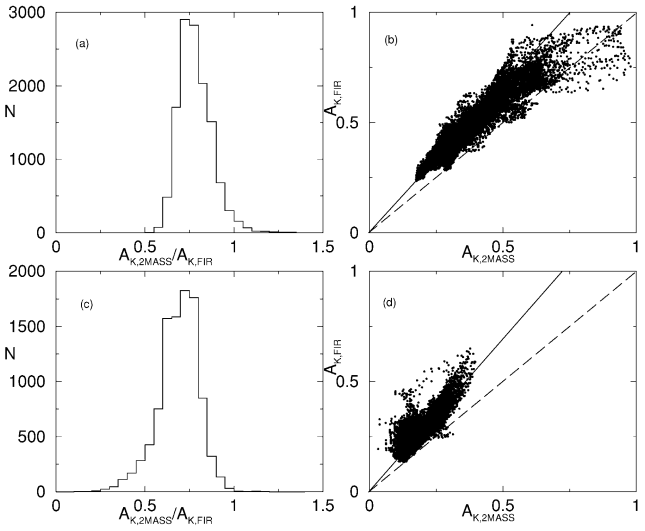

Figure 11. Comparison between $A_{K,\mathrm{2MASS}}$ and $A_{K,\mathrm{FIR}}$ extinction values for cells with $5° > b > 3°$ (upper panels) and $-3° > b > -5°$ (lower panels). Panels (a) and (c) show the $A_{K,\mathrm{2MASS}}/A_{K,\mathrm{FIR}}$ histogram, whereas panels (b) and (d) show the comparison over the entire range in A_K. The dashed lines in the latter panels represent the identity function, whereas the solid lines have angular coefficients equal to the median $A_{K,\mathrm{2MASS}}/A_{K,\mathrm{FIR}}$ value within each strip.

rotation axis. However, it may more readily be explained by a more extended central dust disc hole producing a shadow effect on the ionizing radiation. It would deplete dust grains within a cone, and the ultraviolet (UV) radiation sources are more probably related to continuous star formation in the central parts (e.g. Arches and Quintuplet clusters presently) and/or post-asymptotic giant branch (post-AGB) stars from the central bulge (Binette et al. 1994).

Another way of assessing the effect of dust depletion in the cone region is to show cuts along galactic longitude at different latitudes. This is done in Fig. 10, where we show profiles of $A_{K,\mathrm{2MASS}}$ (solid line) and $A_{K,\mathrm{FIR}}$ (dashed line) along galactic longitude in positions towards the conical structure. We clearly see the effect of central dust depletion in Figs 10(b) and (d), which is not expected at these galactic latitudes.

One could naively argue that $A_{K,\mathrm{2MASS}} < A_{K,\mathrm{FIR}}$ because of dust emission beyond the Galactic centre, which contributes only to $A_{K,\mathrm{FIR}}$. As the relative contribution of background dust should be the major reason for any discrepancy between 2MASS and SFD98 extinction values, we will analyse them separately for three regions, each one divided into a northern and a southern strip: (i) $|\ell| < 5°$ and $5° > |b| > 3°$, (ii) $|\ell| < 5°$ and $3° > |b| > 1°$, and (iii) $|\ell| < 5°$ and $|b| < 0.5°$. This division allows assessment of the correlation between $A_{K,\mathrm{FIR}}$ and $A_{K,\mathrm{2MASS}}$ in regions with varying contributions by the background dust. We hope therefore to disentangle the effect on $A_{K,\mathrm{FIR}}$ by dust on the far side of the Galaxy from other factors that may lead to discrepancies in the $A_{K,\mathrm{FIR}}$ versus $A_{K,\mathrm{2MASS}}$ relation.

4.3.1 Strips $5° > |b| > 3°$

Fig. 11 shows the $A_{K,\mathrm{FIR}}$ versus $A_{K,\mathrm{2MASS}}$ relation in the region $5° > |b| > 3°$. The upper panels correspond to cells in the northern Galactic strip ($|\ell| < 5°$, $5° > b > 3°$), whereas the lower panels correspond to the southern ($|\ell| < 5°$, $-3° > b > -5°$) strip. The $A_{K,\mathrm{2MASS}}/A_{K,\mathrm{FIR}}$ ratio histograms in panels (11a) and (11c) show that the relative extinction values have peaks at 0.75 (75 per cent) and 0.72 (72 per cent) in the northern and southern strips, respectively. These well-defined peaks imply a good linear correlation between the two extinction values, as confirmed in Figs 11(b) and (d). For the northern and southern strips we have the correlations $A_{K,\mathrm{FIR}} = 1.33A_{K,\mathrm{2MASS}}$ and $A_{K,\mathrm{FIR}} = 1.39A_{K,\mathrm{2MASS}}$, respectively, where the angular coefficients were derived from the median $A_{K,\mathrm{2MASS}}/A_{K,\mathrm{FIR}}$ ratio values. In this region, the model predictions indicate that, for both northern and southern strips, the ratio of extinction on foreground of the Galactic to total extinction should be 96 per cent, independent of the Sun's displacement from the disc midplane. From the median $A_{K,\mathrm{2MASS}}/A_{K,\mathrm{FIR}}$ values we infer that a typical value for this ratio is $\approx$ 73 per cent. Therefore, this discrepancy between model and observed extinction ratio suggests that the contribution from background dust cannot explain the observed $A_{K,\mathrm{2MASS}}/A_{K,\mathrm{FIR}}$ ratio.

Arce & Goodman (1999) also found a linear relation between the dust emission extinction and that derived from the stellar content in the Taurus Dark Cloud, with a slope that varies in the range 1.3–1.5. They attributed this difference to the dust column density versus reddening calibration from Schlegel et al. (1998), which may yield an overestimated $A_V > 0.5$. Note that the slopes in our two strips (with $2 > A_V > 10$) are similar to those of Arce & Goodman (1999), which corroborates the idea of a $A_{K,\mathrm{FIR}}$ calibration effect.

We point out that assuming a significantly lower value for R_V would compress the $A_{K,\mathrm{FIR}}$ scale, decreasing the differences between $A_{K,\mathrm{FIR}}$ and $A_{K,\mathrm{2MASS}}$ in Fig. 11. However, observational constraints on R_V do not support this possibility. Indeed, Gould, Stutz & Frogel (2001) estimated $R_{VI} = A_V/E(V-I) = 2.4$ ($R_V \approx 3.0$), from VIK colours of 146 Baade's Window G and K giants. Stanek (1996) obtained $R_{VI} = 2.5 \pm 0.1$ ($R_V = 3.1$), using Baade's Window red clump giants. For stellar fields and reddened metal-rich globular clusters throughout the bulge, values of $R_V = 3.5$–3.6 have been employed (Terndrup 1988; Barbuy et al. 1998). We conclude that typical R_V values in bulge directions cannot be significantly lower than $R_V = 3.1$.

Assuming that the discrepancy between model and observed extinction ratio in these strips is entirely due to a calibration problem, we estimate a calibration factor of 76 per cent to be applied to the $A_{K,\mathrm{FIR}}$ values.

Figs 11(b) and (d) also reveal a strong asymmetry between the northern and southern strips. A_K values reach up to $A_K = 1.0$ in the north, with most cells in the range $0.2 < A_{K,2MASS} < 0.7$. In the south, there are few cells with $A_{K,2MASS} > 0.4$. In Section 4.4, we discuss the north–south asymmetry in more detail.

4.3.2 *Strips* $3^\circ > |b| > 1^\circ$

As we consider regions closer to the Galactic plane, several predictions can be made regarding the extinction values derived from the 2MASS and DIRBE/*IRAS* data. First, one obviously expects a general increase in both $A_{K,2MASS}$ and $A_{K,FIR}$ values. Further, the relation between the two should increasingly depart from the identity line, as the contribution of background dust is enhanced. Finally, line-of-sight variations should also grow in amplitude, as more individual dust clouds, with variable dust densities and temperatures, are expected to lie along low latitude directions.

All these predictions are confirmed by inspection of Fig. 12, which shows the comparison between $A_{K,2MASS}$ and $A_{K,FIR}$ for the region $3^\circ > b > 1^\circ$. The $A_{K,2MASS}/A_{K,FIR}$ histograms in Figs 12(a) and (c) are dominated by double peak distributions, at $A_{K,2MASS}/A_{K,FIR} = 0.75$ and 0.60 for the northern strip, and at $A_{K,2MASS}/A_{K,FIR} = 0.65$ and 0.35 for the southern strip. As a consequence, the $A_{K,FIR}$ versus $A_{K,2MASS}$ relation given in Figs 12(b) and (d) is more complex and not well described by a linear fit. Notice that the double peak nature is clearly seen in Fig. 12(d) as two distinct branches in the $A_{K,FIR}$ versus $A_{K,2MASS}$ relation. The solid lines shown in these panels have angular coefficients derived from the main peak of the $A_{K,2MASS}/A_{K,FIR}$ histograms in Figs 12(a) and (c).

For this region, the model predictions give a foreground to total extinction ratio of 81 per cent. If we artificially introduce in the model the calibration factor obtained for $A_{K,FIR}$ in the previous section, this ratio is reduced to 62 per cent. This is in agreement with the typical $A_{K,2MASS}/A_{K,FIR}$ value found in the two strips. The main peak in the northern strip (with a ratio of 75 per cent) indicates an observed excess of foreground dust with respect to the dust exponential model. The secondary peak in the north matches quite well the calibrated model values. The same applies to the main peak in the southern strip, whose ratio is 60 per cent. The secondary peak in the southern strip (at $A_{K,2MASS}/A_{K,FIR} = 35$ per cent) suggests that the observed $A_{K,FIR}$ is excessively high as compared to the expectations of our simple model. This indicates lines of sight more strongly affected by dense dust clouds and temperature effects caused by dust heated over the DIRBE/*IRAS* temperature correction.

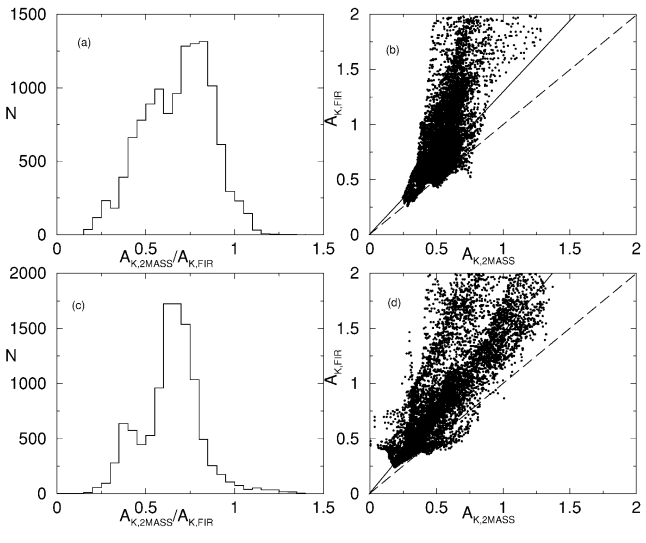

Figure 12. Comparison between $A_{K,FIR}$ extinction values for cells with $3^\circ > b > 1^\circ$ (upper panels) and $-1^\circ > b > -3^\circ$ (lower panels). Panels (a) and (c) show the $A_{K,2MASS}/A_{K,FIR}$ histogram, whereas panels (b) and (d) show the comparison up to $A_K = 2.0$. The dashed lines in the latter panels represent the identity function, whereas the solid lines have angular coefficients equal to the main peak in the corresponding $A_{K,2MASS}/A_{K,FIR}$ histograms.

4.3.3 *Strips* $|b| < 0.5^\circ$

Very close to the Galactic plane, the infrared emission by hot dust near the Centre, across spiral arms or close to star-forming regions, may substantially increase the estimate of $A_{K,FIR}$. Therefore, this latter is expected to deviate significantly from $A_{K,2MASS}$ and to display strong variations due to scatter in line-of-sight dust. Fig. 13 shows $A_{K,FIR}$ versus $A_{K,2MASS}$ for the $|b| < 0.5^\circ$ strips. The $A_{K,2MASS}/A_{K,FIR}$ histograms in Figs 13(a) and (c) show peaks at $A_{K,2MASS}/A_{K,FIR} = 0.27$ (27 per cent) for both northern and southern strips. The models predict a relative extinction of 54 per cent in the same region; introducing the $A_{K,FIR}$ calibration effect found previously, this value changes to 41 per cent. Therefore, the observed extinction ratios are systematically smaller than the model expectations. As discussed in Section 4.2, this is just what one expects from the existence of non-exponential dust distribution (dense dust clouds) in the foreground and background of the Galactic centre, and the overestimation of the $A_{K,FIR}$ due to heated dust. Furthermore, as discussed in the end of Section 2.1, $A_{K,2MASS}$ becomes undetermined for $A_K > 2.5$ due to the limit in the J band optical depth. In fact, this cut-off in the $A_{K,2MASS}$ values is clearly seen in Figs 13(b) and (d), as $A_{K,2MASS}$ saturates for rising $A_{K,FIR}$ values.

4.4 North–south asymmetry

A better way of assessing any north–south discrepancy in the $A_{K,2MASS}$ and $A_{K,FIR}$ data is to directly compare cells with the same value of ℓ but with opposite signs of b. This method has the additional advantage that the comparison is not affected by the incomplete

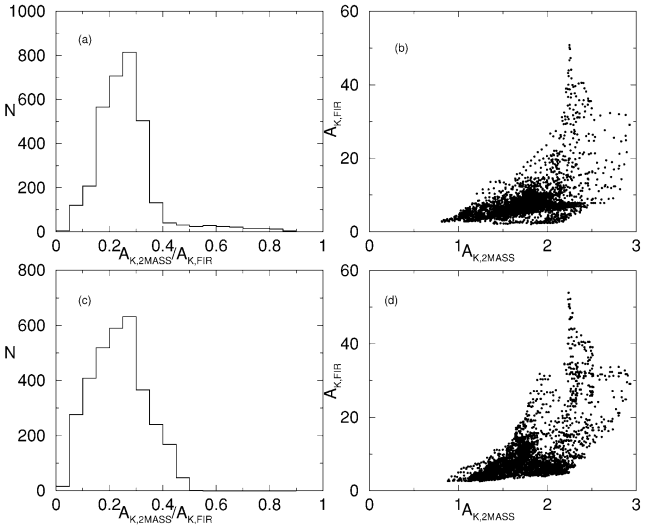

Figure 13. Comparison between $A_{K,2MASS}$ and $A_{K,FIR}$ extinction values for cells with $0^\circ < b < 0.5^\circ$ (upper panels) and $0^\circ > b > -0.5^\circ$ (lower panels). Panels (a) and (c) show the $A_{K,2MASS}/A_{K,FIR}$ histogram, whereas panels (b) and (d) show the comparison over the entire range in A_K.

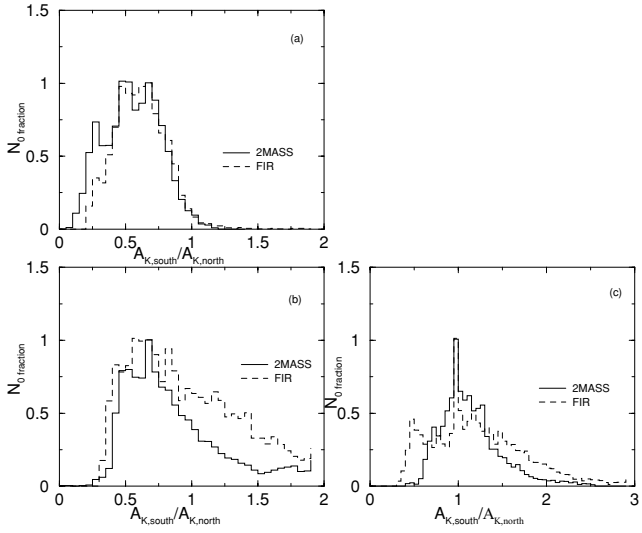

Figure 14. $A_{K,2MASS}$(south)/$A_{K,2MASS}$(north) (solid line) and $A_{K,FIR}$ (south)/$A_{K,FIR}$(north) (dashed line) for cells at $3^\circ < |b| < 5^\circ$ (panel a), $1^\circ < |b| < 3^\circ$ (panel b), and $0^\circ < |b| < 0.5^\circ$ (panel c).

spatial coverage in the southern strip. Fig. 14 shows histograms of the ratio of extinction values in mirror cells relative to the disc plane. Figs 14(a), (b) and (c) present extinction ratios for mirror cells in the strips $3^\circ < |b| < 5^\circ$, $1^\circ < |b| < 3^\circ$ and $0^\circ < |b| < 0.5^\circ$, respectively. The solid histograms in each panel show the distribution of $A_{K,2MASS}$(south)/$A_{K,2MASS}$(north) ratios, while the dashed histograms correspond to the $A_{K,FIR}$(south)/$A_{K,FIR}$(north) distribution.

All histograms are normalized by the main peak in counts, allowing a better comparison. In the region $3^\circ < |b| < 5^\circ$, we have two very similar distributions, with peaks around ≈0.6. The general agreement indicates that both extinction measurements detect the same asymmetry, with the extinction being 60 per cent less in the south than in the north. The strong similarity confirms that, in these particular strips, the extinction measured in the FIR is dominated by dust on the foreground of the stars that were used to measure $A_{K,2MASS}$.

In the region $1^\circ < |b| < 3^\circ$, the observed asymmetry in the FIR and 2MASS data is again very similar in the range $0 < A_{K,south}/A_{K,north} < 0.7$, displaying a large peak centred around 0.6 (60 per cent). However, the FIR ratios are systematically larger than the 2MASS one in the $A_{K,south}/A_{K,north} > 0.7$ domain. This indicates a systematic trend in the sense that southern cells suffer a more significant contribution by background dust than their corresponding mirror cells in the north.

In the region $|b| < 0.5^\circ$, the north–south asymmetry is substantially reduced and, interestingly enough, most cases now have $A_{K,south}/A_{K,north} \approx 1.0$. This applies to both FIR and 2MASS data, the main difference between the two data sets being the larger dispersion in the south/north values in the former relative to the latter.

Interpreting this north–south asymmetry is not an easy task. The similarity of the histograms in Fig. 14(a) plus our model predictions suggest that extinction in the $3^\circ < |b| < 5^\circ$ strips is dominated by foreground structure in the form of extended dust clouds (see also map in Fig. 3 and the concluding section). At lower latitudes, the extinction values increase and become dominated by diffuse dust distribution or by dense clouds located close to the Galactic centre. In these cases, the shape and position of the $A_{K,south}/A_{K,north}$ histograms in both data sets should reflect the global properties of the dust distribution rather than the contribution of any individual dust cloud. As the FIR data reach deeper into the dust columns than the 2MASS, the transition from the foreground dominated regime to one dominated by the global distribution starts earlier in the former data set; this effect is the likely cause of the difference in the histograms in Fig. 14(b).

In the $|b| < 0.5^\circ$ strip, the $A_{K,2MASS}$ values are strongly limited by optical depth and largely unreliable (Section 2.1), while the $A_{K,FIR}$ values are suffer from the effects of dust heated beyond 21 K. Despite these uncertainties the dust distribution in this region is reasonably symmetric. There is a small trend in the sense of $A_{K,south}/A_{K,north} > 1$, especially in the FIR data. This trend is intriguing. The fact that most cells have larger $A_{K,FIR}$ values at southern latitudes than at northern ones may be telling us something about the geometry of the dust distribution relative to the Sun's position.

In order to take into account a possible displacement by the Sun relative to the disc mid-plane, we again use our model presented in Section 4.1. Considering the Sun displaced by 5, 15 and 25 pc above the plane, we obtain typical south/north ratios in the $\tau_{8.5}$ or τ_∞ values of 1.08, 1.27 and 1.50, respectively. However, the model does not incorporate any asymmetry caused by foreground dust clouds, which seems to be the dominant effect generating the asymmetry in the 2MASS and FIR data. It is thus impossible at the present to quantify the Sun's displacement from the disc based on the data. We should point out that Unavane et al. (1998), using DENIS data, also concluded that the asymmetry in the inner bulge extinction is dominated by foreground dust clouds.

5 CONCLUDING REMARKS

We built the A_K extinction map towards the central $10^\circ \times 10^\circ$ of the Galaxy using the 2MASS Point Source Catalog. We extracted J and K_s magnitudes for about 6×10^6 stars in the range $8.0 \leqslant K_s \leqslant 13.0$. The adopted map resolution is 4×4 arcmin^2. It was possible to obtain extinction values for ≈80 per cent of the 32 761 cells defined in the area, where 2MASS data were currently available and a bulge giant branch was distinct enough. The extinction affecting the bulk of the bulge stellar population was determined by matching the upper giant branch found in the K_s, $(J-K_s)$ colour–magnitude diagram to the reference upper giant branch, which was built using de-reddened bulge fields. The extinction values vary from $A_K = 0.05$ in the edges of the map up to $A_K = 3.2$ close to the Galactic centre. The mean extinction found is $\langle A_K \rangle = 0.29$ with a dispersion $\sigma = 0.12$; 63 per cent of the cells are within 2σ of the mean.

We compared our 2MASS extinction map to that of Schultheis et al. (1999) in the region $|\ell| < 5^\circ$ and $|b| < 1.5^\circ$, which is common to both studies. Schultheis et al. extinction map is based on DENIS photometry. We find an excellent agreement between the two extinction determinations, especially up to $A_K = 1.0$. Beyond this limit the values derived from the DENIS data are systematically larger. This small discrepancy in large extinction regions is not unexpected, considering the photometric errors, incompleteness effects and uncertainties in extinction determination.

We also compared the present extinction map to that of Schlegel et al. (1998), which is based on dust emission in the FIR detected by the DIRBE/*IRAS* instruments. As the data from the latter are affected by the entire dust column, with no depth limit, the comparison was made separately for regions of decreasing Galactic latitude b, which supposedly correspond to increasing contribution by dust located on the background of the Galactic centre. The background dust contribution was estimated by means of a double exponential dust distribution model. Some expected systematic biases, besides that

caused by dust on the far side of the Galaxy, were also assessed and quantified.

In general, the extinction values derived from dust emission are higher than those from 2MASS, mainly close to the Galactic plane and centre. We detected two unexpected regions symmetric and close to the Galactic centre where the two extinction estimates are of the same order. The lack of background dust in these low latitude regions could be explained by a process of dust grain destruction by UV emission from sources associated with continuous star formation and/or post-AGB stars in the central parts of the Galaxy.

For the cells in the region $3^\circ < |b| < 5^\circ$, we observe a clear and roughly linear correlation between the A_K values from 2MASS and dust emission. We also confirm, as was done in Paper I, that the A_K values from 2MASS data are in general 73 per cent smaller than those derived from dust emission. As in this region the background dust contribution is less than 5 per cent, the differences between these two quantities should be smaller than observed. This discrepancy is also verified by Arce & Goodman (1999) in the Taurus Dark Cloud. It is probably due to systematic effects in the dust column density versus reddening calibration from Schlegel et al. (1998), yielding an overestimate of extinction in moderate to high extinction regions. We estimate a calibration correction factor of 76 per cent for the FIR extinction values.

For the intermediate $1^\circ < |b| < 3^\circ$ region, the relation between DIRBE/*IRAS* and 2MASS extinction values departs more significantly from the identity line, as expected due to the larger contribution by background dust. In this region, the typical $A_{K,\mathrm{2MASS}}/A_{K,\mathrm{FIR}}$ ratio is 65 per cent and could be explained by background dust contribution and the calibration factor affecting the FIR data. An enhancement in the foreground dust with respect to the dust model is observed in many cells in the northern strip. In the southern strip, several cells have $A_{K,\mathrm{2MASS}}/A_{K,\mathrm{FIR}}$ smaller than expected, probably due to dense dust clouds and temperature variations, currently not incorporated into our model.

For the regions very close to the Galactic plane ($|b| < 0.5^\circ$), we have a typical value for the $A_{K,\mathrm{2MASS}}/A_{K,\mathrm{FIR}}$ ratio of 27 per cent. Even considering the background dust contribution and the calibration factor, this ratio is still smaller than that predicted by our simple model for the dust distribution. This fact is probably due to the overestimation of the $A_{K,\mathrm{FIR}}$ values by heated dust above that obtained from DIRBE temperature maps. Another possible contribution to this difference is the existence of systematic effects on the $A_{K,\mathrm{2MASS}}$ values in high extinction regions ($A_{K,\mathrm{2MASS}} > 2.5$), where the 2MASS extinction should be significantly underestimated or even unreliable.

A systematic asymmetry in the A_K values relative to the plane of the Galaxy at $1^\circ < |b| < 5^\circ$ is observed both in the 2MASS and DIRBE/*IRAS* data. The behaviour and amplitude of this asymmetry with position on the sky suggest that the dominant role in creating this north–south asymmetry is a more effective presence of foreground dust clouds in the northern Galactic strips, such as the Pipe Nebula (Section 2.2). A possible explanation is stellar winds and supernovae from nearby OB stellar associations producing dust cloud shells (Bhatt 2000). The nearby clouds projected towards the central parts of the Galaxy at positive latitudes belong to the Ophiuchus dust complex. They are probably related to the association ScoOB2, which is at a distance of 145 pc from the Sun (Bhatt 2000; Onishi et al. 1999). ScoOB2, in turn, belongs to Upper Scorpius, which is the easternmost part of the Sco-Cen Association, as studied by means of *Hipparcos* (de Zeeuw et al. 1999).

In all regions, significant substructure in the $A_{K,\mathrm{2MASS}}$ versus $A_{K,\mathrm{FIR}}$ relation is seen, with loops and arms stretching out from the main relation. These structures are probably caused by intervening dust clouds, with different temperatures and densities for different lines of sight. One extremely interesting perspective is to model the dust distribution within the Galaxy, trying to reproduce as closely as possible the details of the A_K maps currently available. This effort demands models that incorporate, on top of a smooth dust distribution, the effects of individual dust clouds, spiral arms, molecular rings and other structure, possibly with variable density contrasts and temperatures. This effort is currently under way for the central region of the Galaxy.

ACKNOWLEDGMENTS

This publication makes use of data products from the Two Micron All Sky Survey, which is a joint project of the University of Massachusetts and the Infrared Processing and Analysis Centre/California Institute of Technology, funded by the National Aeronautics and Space Administration and the National Science Foundation. We also use the electronic form of the extinction maps provided by Schultheis et al. (1999) and Schlegel et al. (1998). We thank the anonymous referee for his/her interesting comments and suggestions. We acknowledge support from the Brazilian institutions FAPESP and CNPq. CMD acknowledges FAPESP for a postdoctoral fellowship (proc. 00/11864-6).

REFERENCES

Arce H. G., Goodman A. A., 1999, ApJ, 512, L135
Baade W., 1963, Evolution of Stars and Galaxies. Harvard Univ. Press, Cambridge MA, p. 277
Barbuy B., Bica E., Ortolani S., 1998, A&A, 333, 117
Barbuy B., Ortolani S., Bica E., Desidera S., 1999, A&A, 348, 783
Bertelli G., Bressan A., Chiosi C., Fagotto F., Nasi E., 1994, A&AS, 106, 275
Binette L., Magris C. G., Stasinska G., Bruzual A. G., 1994, A&A, 292, 13
Bhatt H. C., 2000, A&A, 362, 715
Cardelli J. A., Clayton G. C., Mathis J. S., 1989, ApJ, 345, 245
Catchpole R. M., Whitelock P. A., Glass I. S., 1990, MNRAS, 247, 479
Cohen M., 1995, ApJ, 444, 874
de Zeeuw P. T., Hoogerwerfet R., de Bruijne J. H. J., Brown A. G. A., Blaauw A., 1999, AJ, 117, 354
Drimmel R., Spergel D. N., 2001, ApJ, 556, 181
Dutra C. M., Santiago B. X., Bica E., 2002, A&A, 381, 219
Epchtein N. et al., 1997, The Messenger, 87, 27
Frogel J. A., Tiede G. P., Kuchinski L. E., 1999, AJ, 117, 2296 (FTK99)
Gould A., Stutz A., Frogel J. A., 2001, ApJ, 547, 590
Hammersley P. L., Garzon F., Mahoney T., Calbet X., 1995, MNRAS, 273, 206
Mendez R. A., van Altena W. F., 1998, A&A, 330, 910
Ramírez S. V., Stephens A. W., Frogel J. A., DePoy D. L., 2000, AJ, 120, 833
Robin A. C., Haywood M., Crézé M., Ojhan D. K., Bienayme D., 1996, A&A, 305, 125
Schlegel D. J., Finkbeiner D. P., Davis M., 1998, ApJ, 500, 525 (SFD98)
Schultheis M. et al., 1999, A&A, 349, L69
Skrutskie M. et al., 1997, in Garzon F., Epchtein N., Omont A., Persi P., Burton B. eds, The Impact of Large Scale Near-IR Sky Surveys. Kluwer, Dordrecht, p. 25
Stanek K. Z., 1996, ApJ, 460, L37
Storchi-Bergmann T., Bonatto Ch. J., 1991, MNRAS, 250, 138
Terndrup D. M., 1988, AJ, 96, 884
Unavane M., Gilmore G., Epchtein N., Simon G., Tiphene D., de Batz B., 1998, MNRAS, 295, 119

This paper has been typeset from a TEX/LATEX file prepared by the author.